Ab initio study of electron paramagnetic resonance hyperfine structure of the silicon dangling bond: Role of the local environment

Gernot Pfanner, Christoph Freysoldt, and Jörg Neugebauer
Max-Planck-Institut für Eisenforschung GmbH, D-40237 Düsseldorf, Germany
(Received 6 January 2011; revised manuscript received 17 March 2011; published 22 April 2011)

The hyperfine coupling of the electron spin to the nuclear spins nearby contains information on the local environment such as the chemical composition, distances, or bond angles. A correct interpretation of this information requires a comparison to a theoretical model. In this work, we employ spin-density-functional theory and *ab initio* pseudopotentials to study how the hyperfine couplings of a Si dangling bond change under systematic variations of the local environment. For our network models, which take the effect of the extended host into account (supercell approach), we show that the hyperfine tensor of the undercoordinated silicon atom is governed by the interplay between *s*-*p* hybridization and the degree of localization of the defect state.

DOI: 10.1103/PhysRevB.83.144110 PACS number(s): 76.30.−v, 71.15.Mb, 71.55.Cn

I. INTRODUCTION

Electron paramagnetic resonance (EPR) is a powerful experimental technique to study point defects in solids.[1–4] The spectrum, which results from flipping the spin of unpaired electrons in an external magnetic field, yields information on the symmetry of the defect structure as well as on the type of atoms involved. Much of the structural information stems from the hyperfine interaction between the unpaired electron spin and the spin of nearby nuclei. The so-called superhyperfine interaction, which arises from the interaction between the electron and nuclei of the lattice surroundings, yields further insights into the structure of the defect.

However, to derive a microscopic picture of the defect from the experimental data requires knowledge of the defect wave function. For example, it is not possible to derive the distance between a particular nucleus and the defect center from the superhyperfine splitting in the spectrum alone. Such information can only be obtained by comparison to theoretical calculations of an EPR spectrum for a given defect. For that purpose, various approaches with different levels of sophistication exist. Semiempirical methods based on the linear combination of atomic orbitals (LCAO) have been successfully used to explain trends in the EPR spectra, but their accuracy is often insufficient for direct comparison with experiment. More reliable methods based on all-electron calculations are usually limited by the size of the system. A powerful approach to circumvent both deficiencies consists in utilizing spin-density-functional theory and *ab initio* pseudopotentials.[5]

The EPR technique has been extensively applied to study paramagnetic defects in crystalline silicon[4] (*c*-Si). Prominent examples are the P_b center[6–8] (a dangling bond at a Si-SiO_2 interface) and the negatively charged vacancy.[9,10] Similarly, it can be used for investigating the mechanisms behind the light-induced degradation of solar cells based on hydrogenated amorphous silicon[11,12] (*a*-Si:H). However, in this case the interpretation of the experimental data is challenging due to significant deviations from the crystalline structure. Consequently, a profound knowledge of the influence of the local geometry [see Fig. 1(a)] on the EPR parameters is required. However, this aspect has only been investigated by theoretical studies on small clusters so far[13–15] that largely neglect the influence of the extended host's electronic structure.

There is an absence of systematic work, in which the presence of an extended host material is taken into account. Consequently, we have carried out first-principles supercell calculations to reveal how changes in the structure surrounding the defect affect the hyperfine interaction. To disentangle structural effects of the local defect environment from the rest of the material, we consider dangling-bond (db) models based on *c*-Si.

The paper is organized as follows. In the next section, we briefly summarize the theoretical scheme to compute hyperfine parameters in a pseudopotential approach. After that, we describe db models in *c*-Si, and proceed with a description of the employed methods in Sec. III. In the final section, we present and discuss our results.

II. THEORETICAL APPROACH

The hyperfine interaction characterizes the interaction between the magnetic moment of the unpaired electron or hole and the magnetic moments of the nuclei. The corresponding Hamiltonian for coupling to a single nucleus is given by $H = \mathbf{I} \cdot \mathbf{A} \cdot \mathbf{S}$, where $\mathbf{I}$ and $\mathbf{S}$ stand for the electron and nuclear spin, respectively. The hyperfine tensor $\mathbf{A}$ can be decomposed into an isotropic and an anisotropic part,[2]

$$A_{ij} = a\delta_{ij} + B_{ij}, \tag{1}$$

where a and B_{ij} denote the Fermi contact interaction and the traceless anisotropic hyperfine tensor, respectively.

The Fermi contact interaction is given in the nonrelativistic limit by

$$a = \frac{2\mu_0}{3} g_e \mu_e g_I \mu_I \cdot \rho_S(\mathbf{R}), \tag{2}$$

where μ_0 is the permeability in vacuum, g_e is the electron g factor, μ_e is the Bohr magneton, and g_I and μ_I are the gyromagnetic ratio and nuclear magneton of the nucleus. We note that the gyromagnetic ratio of Si is negative, and therefore also the hyperfine couplings to the majority spin in our calculations are negative numbers. However, standard

EPR experiments can only probe the absolute value of a, and therefore in these publications it is commonly given as a positive number.

The spin density in Eq. (2), $\rho_S(\mathbf{r}) = \rho_\uparrow(\mathbf{r}) - \rho_\downarrow(\mathbf{r})$, depends solely on the position $\mathbf{R}$ of the nucleus. Since only the s-wave function, i.e., $l = 0$, is nodeless at $\mathbf{R}$, this parameter consequently characterizes the s-like character of a system. In a first-order scalar-relativistic treatment, $\rho_S(\mathbf{R})$ has to be replaced by an average over a small sphere around the nucleus with a radius on the order of the Thomson radius[16] $r_{\mathrm{Th}} = Ze^2/mc^2 \approx 5Z \times 10^{-5}$Bohr ($Z$ is the nuclear charge, e is the elementary charge, m is the electron mass, and c is the speed of light),

$$\rho_S(\mathbf{R}) \to \langle \rho_{\mathrm{Th}} \rangle(\mathbf{R}) = \int \delta_{\mathrm{Th}}(|\mathbf{R} - \mathbf{r}|)\rho_S(\mathbf{r})d^3r, \tag{3}$$

with $\delta_{\mathrm{Th}}(r)$ defined by

$$\delta_{\mathrm{Th}}(r) = \frac{1}{4\pi r^2} \frac{r_{\mathrm{Th}}/2}{[(1 + E/2mc^2)r + r_{\mathrm{Th}}/2]^2}, \tag{4}$$

where E denotes the nonrelativistic energy.

The anisotropic tensor[2]

$$B_{ij} = \frac{\mu_0}{4\pi} g_e \mu_e g_I \mu_I \int \frac{3r_i r_j - \delta_{ij} r^2}{r^5} \cdot \rho_S(\mathbf{r}) d\mathbf{r} \tag{5}$$

stands for a magnetic dipole-dipole interaction between electron and nucleus at the relative distance $\mathbf{r}$. Indeed, for a δ-like spin density, the classical point dipole-dipole interaction can be obtained.

The tensor is in its principal system described by two anisotropic interaction constants,[1] namely the uniaxiality b and the asymmetry (rhombicity) parameter c. Assuming that the eigenvalues of B are sorted according to $|B_1| \leqslant |B_2| \leqslant |B_3|$, the parameters are defined by

$$b = \frac{B_3 - (B_2 + B_1)/2}{3}, \tag{6}$$

$$c = \frac{|B_2| - |B_1|}{2}. \tag{7}$$

Both parameters vanish for systems with cubic symmetry and are, in contrast to a, only available upon diagonalization of $\mathbf{A}$. The c parameter becomes zero for systems with axial symmetry, for which two principal values coincide. This is also the case for the systems under investigation here. The b parameter can be also expressed as the scalar product of a spherical harmonics with $l = 2$ and the spin density.[5] This way, it becomes clear that the parameter projects out the d-like component of the spin density, thus the anisotropy b probes for the local p character of the singly occupied wave function in sp-bonded systems like silicon. [The maximum l component $l_{\max}$ of the density $\rho(r)$ and the generating wave function $\psi(r)$ fulfill the condition $l_{\max}^{\rho(r)} \leqslant 2l_{\max}^{\psi(r)}$ if $\rho(r) = |\psi_s(r)|^2$.]

The computation of Eqs. (2) and (5) requires knowledge of the spin density $\rho_S(\mathbf{r})$, which can be obtained from density-functional theory.[17,18] For the computation of defects in large systems, it is convenient to use pseudopotentials,[19] so that the core electrons are removed from the calculation and the valence electrons are described by nodeless wave functions. However, since the hyperfine parameters depend crucially on the core region, it becomes necessary in this case to reconstruct the wave function inside this region from that obtained from a pseudopotential calculation. Several schemes[5,20,21] have been proposed for this purpose. In this work, we employ the single-projector method[5] to calculate the hyperfine parameters, which has been implemented into the DFT library S/PHI/nX.[22]

III. COMPUTATIONAL METHODS

A. Dangling-bond models

We shall see in the following that the hyperfine couplings of the Si atom, where the dangling-bond state resides, are determined by two major effects, namely s-p hybridization and spin delocalization. The hybridization state is closely linked to the atomic geometry, i.e., the bond angle α at the dangling bond (Fig. 1). In a planar configuration ($\alpha = 120°$), the Si-Si bond orbitals are sp^2 hybrids, while the db orbital is a pure p state. At the tetrahedral angle ($\alpha = 109.5°$), the backbond orbitals and the db orbital are equivalent sp^3 hybrids (25% s, 75% p). The second important effect is the localization of the db state. Even though we discuss it in terms of a local orbital at the db atom, the true electronic eigenstate decays

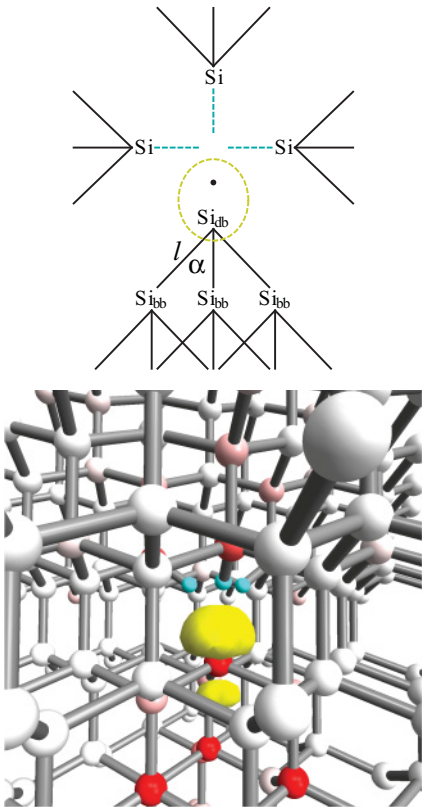

FIG. 1. (Color online) (a) Sketch of the vacancy in crystalline silicon. To arrive at a single dangling bond (indicated by the dashed circle), one has to remove the other three electrons (dashed lines) from the vacancy, e.g., by passivating those bonds with hydrogen as it is done in (b). Next neighbors of the db atom are called backbonds (bb). The bond angle $\mathrm{Si_{bb}} - \mathrm{Si_{db}} - \mathrm{Si_{bb}}$ is denoted by α and l stands for the bond length $\mathrm{Si_{db}} - \mathrm{Si_{bb}}$. (b) Spin density of a dangling bond in a hydrogen-passivated vacancy. The hydrogen atoms are the smaller spheres, colored turquoise. Only the dark, red-colored silicon atoms show a significant isotropic hyperfine coupling.

exponentially into the bond network that hosts the dangling bond. The decay constant and thus the contribution of the delocalized exponential tail to the norm depends on the energetic position of the db state. If it is energetically close to the network states, i.e., the valence or conduction band of silicon, it will strongly hybridize with these and become more delocalized. Delocalization reduces the hyperfine coupling to the db nucleus and nearby atoms, while the superhyperfine couplings to distant atoms are enhanced. This effect is largely absent in small cluster models[13–15] (like molecules), since the quantum confinement increases the gap between occupied and unoccupied states. Consequently, network structural models are required to study the influence of this effect.

For the systematic study of the dependence of the hyperfine parameters on the bond parameters of the local db environment, we consider small molecular radicals (silyl [SiH_3] and tetrasilyl [Si_4H_9]) and various db models in crystalline silicon. In the latter case, there are several possibilities to create a localized dangling-bond state that can contain an unpaired electron. One way consists in passivating vacancies with hydrogen (Fig. 1). We have considered two of this kind, namely the smallest vacancy $V(SiH)_3$ [the neighboring atoms of the vacancy are given in brackets] and a larger one $V_4(SiH)_9$. Another possibility of creating a dangling bond in silicon is to replace neighbors by impurities, which chemically bind the excessive electrons, e.g., by phosphorus $V(P_3)$ or aluminum $V(Al_2SiH)$ [we exclude the fully Al-substituted vacancy $V(Al_3)$ since the hybridization with Al states completely destroys the dangling-bond character of the orbital of interest]. Finally, we have considered a dangling bond on a H-passivated Si(111) surface, which corresponds to the extreme case in which there are no atoms opposite to the db atom [this can be thought of as removing all layers above the db atom in Fig. 1(b)].

To decouple the dependence of bond angle and bond length, we have used the following atomic relaxation schemes. For the bond length we only consider the tetrasilyl radical. To vary the bond length, we move the three SiH_3 groups bound to the db atom along the bond direction for three different bond angles. For the bond-angle dependence, we first displace the db atom from its lattice position. Then we only relax the backbond atoms, so that the bond length is recovered within 8% of the relaxed value. This scheme is carried out for all models at the ideal lattice structure to make the comparison independent of other structural effects. Only the hydrogen atoms are relaxed to recover the correct Si-H bond length to ensure that the corresponding bonding states are well below the valence-band edge.

To study the superhyperfine interaction opposite to the db atom, we consider two larger hydrogenated vacancies originating from removing two or three silicon atoms. Again, we only relax the hydrogen atoms to preserve the overall geometry of the models.

B. Parameters

The DFT calculations employ a plane-wave basis set and norm-conserving pseudopotentials as implemented in the S/PHI/nX code.[22] The plane-wave energy cutoff E_C is set to 40 Ry. As already mentioned in the original article,[5] one observes a strong sensitivity of the a parameter on E_C, which can be improved by rescaling the density at the nucleus with the one of the isolated atom. In this work, we employ the local-spin-density approximation.[23] The choice of the exchange-correlation functional was found to exert a minor influence on the results in the cases studied so far,[24–26] but nevertheless we have checked that all trends can be reproduced with the Perdew-Burke-Ernzerhof (PBE) functional.[27]

The norm-conserving pseudopotentials are generated with the FHI98PP code,[19] where we choose Hamann-type[28] with default values. We also include scalar-relativistic effects for the isotropic parameter, which requires the correction of the atomic all-electron density in the original scheme[5] $|\phi_s(0)|^2$ according to Eq. (3). For the computation we proceed as follows. The s-wave function diverges for $r \to 0$ like $\phi_s(r) = Cr^{\lambda-1}$, where $\lambda = \sqrt{1-\alpha^2 Z^2}$ with $\alpha = 1/137$. The constant C can be obtained from the condition that $\phi_s(r_0)$ coincides with the corresponding solution $\psi_s(r_0)$ computed by the FHI98PP program at the minimal grid point r_0. The integration with the smeared δ function $\delta_{\mathrm{Th}}(r)$, according to Eq. (3), can be rewritten as

$$\int_0^\infty |\psi_s(r)|^2 \delta_{\mathrm{Th}}(r) r^2 dr = \int_0^\infty |\phi_s(r)|^2 \delta_{\mathrm{Th}}(r) r^2 dr + \int_{r_0}^{r_{\max}} \{|\psi_s(r)|^2 - |\phi_s(r)|^2\} \delta_{\mathrm{Th}}(r) r^2 dr. \quad (8)$$

The first integral is computed analytically, the second one numerically on the standard logarithmic grid. This approach ensured that the results converge as $r_0 \to 0$.

To check the accuracy of our approach, we have performed test calculations on two silyl radicals and compared the results with an all-electron method. For the latter, we use GAUSSIAN03 (Ref. 29) with the local-spin-density approximation. To ensure convergence with respect to the Gaussian basis set, we employ an uncontracted WTBS basis set for silicon and the EPR-III basis set for hydrogen, and a Douglas-Kroll-Hess zero-order relativistic Hamiltonian. (An interesting observation concerns the inclusion of relativistic effects in the all-electron calculation. It changes the isotropic value significantly, namely by 30% with respect to a nonrelativistic calculation.). For comparison, we take the structure obtained from the GAUSSIAN03 calculation and compute the hyperfine parameters with our pseudopotential method. (However, the differences of structure relaxation between GAUSSIAN03 and S/PHI/nX are rather insignificant: the bond angle just differs by 0.2% and the bond length by 0.35%.) The corresponding results are reported in Table I. For the a parameter, the pseudopotential approach yields lower values than the all-electron approach. On the

TABLE I. Comparison of hyperfine parameters (in MHz) between GAUSSIAN03 and S/PHI/nX for two silyl radicals (Δ denotes the difference between both methods).

	(MHz)	G03	S/PHI/nX	Δ
SiH_3	a	−649	−635	+2%
	b	−88	−98	−11%
Si_4H_9	a	−346	−310	+10%
	b	−82	−87	−6%

other hand, the b parameter is overestimated compared to GAUSSIAN03. From these examples we see that the absolute accuracy of our scheme is on the order of 10% for both parameters. The discrepancy can be partly explained by polarization of the core electrons, which is not taken into account in our pseudopotential approach. However we have carefully checked that trends for bond parameter variations are reproduced correctly independently of the computational details.

The calculations for the dangling bond in crystalline silicon are carried out in a $2 \times 2 \times 2$ supercell and 16 atomic layers for the surface, respectively (64 Si atoms without the defect). The Brillouin zone integration is done on a $3 \times 3 \times 3$ Monkhorst-Pack mesh[30] with $k = [1/2,1/2,1/2]$ (for the surface, $k = [1/2,1/2,1/4]$) as the generating point. For the bond-angle dependence we use an electronic temperature $kT = 0.025$ eV (room temperature) to reduce the occupational effects for the case in which the defect band hybridizes with bulk states. (Defect dispersion effects are averaged out by integrating over the Brillouin zone with constant occupation. However, defect resonances below the topmost bulk state are erroneously occupied. As done in this work, this effect can be reduced by partial occupations obtained from Fermi smearing.) To minimize artifacts from the dispersion of the defect band, we keep the spin moment fixed. The supercell convergence has been cross-checked for the db models with a $3 \times 3 \times 3$ supercell (216 Si atoms) and we found deviations less than 6% for the a parameter and 4% for the b parameter. For the superhyperfine coupling, we consider $3 \times 3 \times 3$ supercells to minimize supercell artifacts.

IV. RESULTS

A. Bond length

In the following, we will discuss the influence of the bond length between the dangling-bond atom and its three backbond neighbors. To decouple the effect of this parameter from that of the bond angle, we focus on the tetrasilyl molecule. In this case, the bond length can be easily varied by displacing the SiH_3 groups along the bond direction. We do this for three characteristic bond angles: the tetrahedral (109.5°), the relaxed one (116°), and the planar one (120°). The results are shown in Fig. 2. When the bond length is changed from its relaxed value 2.30 Å by ±10%, which reflects the bond-length variations in amorphous silicon,[31] we obtain an essentially linear trend for the isotropic parameter for all bond angles. This dependence of a of the bond length l (in Å) can be characterized by

$$a(l) = a_0 + k(l - l_0), \tag{9}$$

where $l_0 = 2.3$ Å is the equilibrium bond length, $k = -181, -163$, and -122 MHz, and $a_0 = -509$, -291, and -129 MHz, respectively, for the bond angles $\alpha = 109.5°, 116°$, and 120°. The magnitude increases from 120° to 109.5° in accordance with the increasing s character of the db orbital. For the dipolar coupling, the dependence varies from linear at 120° to almost parabolic at 109.5°, but the overall effect is small (±5 MHz). For completeness, we note that for dramatic variations of the bond length (bond breaking) an additional spin-delocalization mechanism comes into play.[32]

B. Bond angle

To study the influence of the bond angle on the hyperfine parameters, we have carried out the relaxation scheme described in Sec. III A. In principle, the accompanied variation of the bond length is not negligible, but we have checked that the magnitude of the bond-angle variation effect is qualitatively independent of the other bond parameter.

The bond angle α determines the s-p hybridization at the dangling-bond center. Since the db orbital becomes purely p-like for 120°, we expect an increase of the dipolar coupling b and a decrease of the isotropic coupling with increasing α. This is indeed observed for the tetrasilyl molecule, but significant deviations occur for the crystalline db models (Fig. 3). For small bond angles, both hyperfine parameters decrease, indicating a delocalization of the spin away from the dangling-bond atom. This can be rationalized as follows. The variation of the bond angle does not only influence the s-p hybridization but it also affects the energetic position of the dangling-bond level. With respect to a pure p orbital, an admixture of s character implies a lower energy. However, as the db level approaches the valence-band edge, it starts to hybridize and delocalize as described in Sec. III A. At which angle this occurs depends on the original position of the state in the relaxed configuration and thus on the chemical environment of our models. Electronegative elements such as phosphorus raise the db level due to Coulomb repulsion, and thus the delocalization comes into play only at small bond angles. Electropositive elements like aluminum, on the other

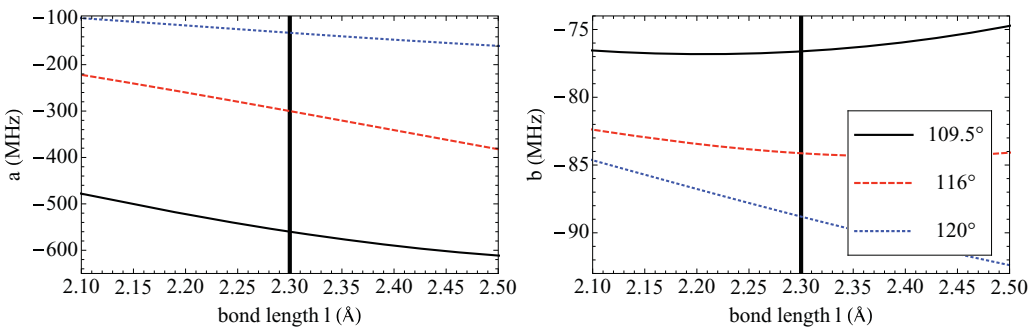

FIG. 2. (Color online) Dependence of the hyperfine parameters on the variation of the bond length for the Si_4H_9 molecule. Three different bond angles are considered, namely tetragonal (109.5°), relaxed 116°, and planar 120°. The vertical line marks the relaxed bond length.

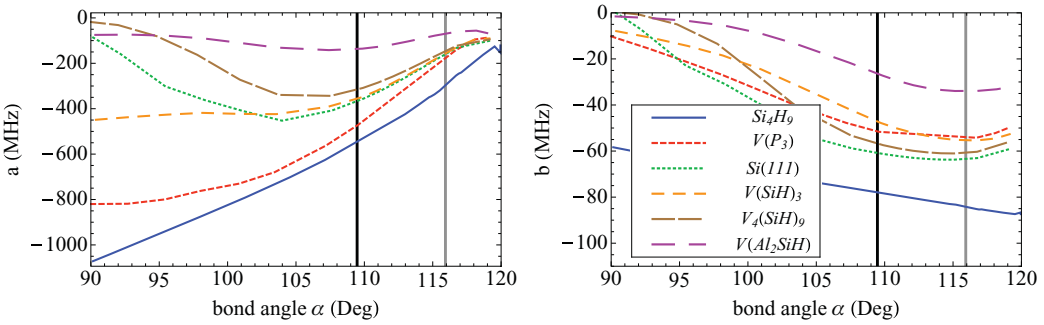

FIG. 3. (Color online) Dependence of the hyperfine parameters on the variation of the bond angle for the Si_4H_9 molecule and the c-Si db models. The black line marks the bond angle of the c-Si db models and the gray line marks that of the Si_4H_9 molecule, respectively.

hand, pull the level close to the valence band. Therefore, the singly occupied level is delocalized already for bond angles slightly below 120°. This effect can be easily monitored for the partial density of states

$$D(E) = \int \sum_n \delta(E - \varepsilon_n(\mathbf{k})) \sum_{i=s,p} |\langle \psi_n(\mathbf{k}) | \phi_i \rangle|^2 d\mathbf{k}, \quad (10)$$

where $\psi_n(\mathbf{k})$ and $\epsilon_n(\mathbf{k})$ correspond to the wave functions and eigenvalues obtained from the pseudopotential calculation, and ϕ_i to projector functions constructed from the atomic partial waves.[5]

In practice, the integral in Eq. (10) is replaced by a sum and the δ function by a Gaussian (broadening 0.1 eV). For our spin-polarized calculations, we plot the spin-resolved density of states $D^{\uparrow}$ (majority spin) and $-D^{\downarrow}$ (minority spin) into a single graph. Figure 4 shows the partial density of states for three characteristic models for three bond angles. One can clearly see the downshift of the defect levels with decreasing bond angle for the $V(P_3)$ and the $V_4(SiH)_9$ db model. If the level falls below the valence-band maximum due to the chemical environment, i.e., for the $V(Al_2SiH)$ model, the features are broadened and ultimately disappear.

In an *ab initio* study on small clusters,[14] it has already been shown that the empirical LCAO picture is not accurate enough to distill the bond-angle range[12] from the hyperfine interaction. However, cluster models cannot capture the effect of delocalization due to the width of the band gap and the small numbers of neighbors. Since we are not restricted by these effects, it is elucidating to consider the relationship between

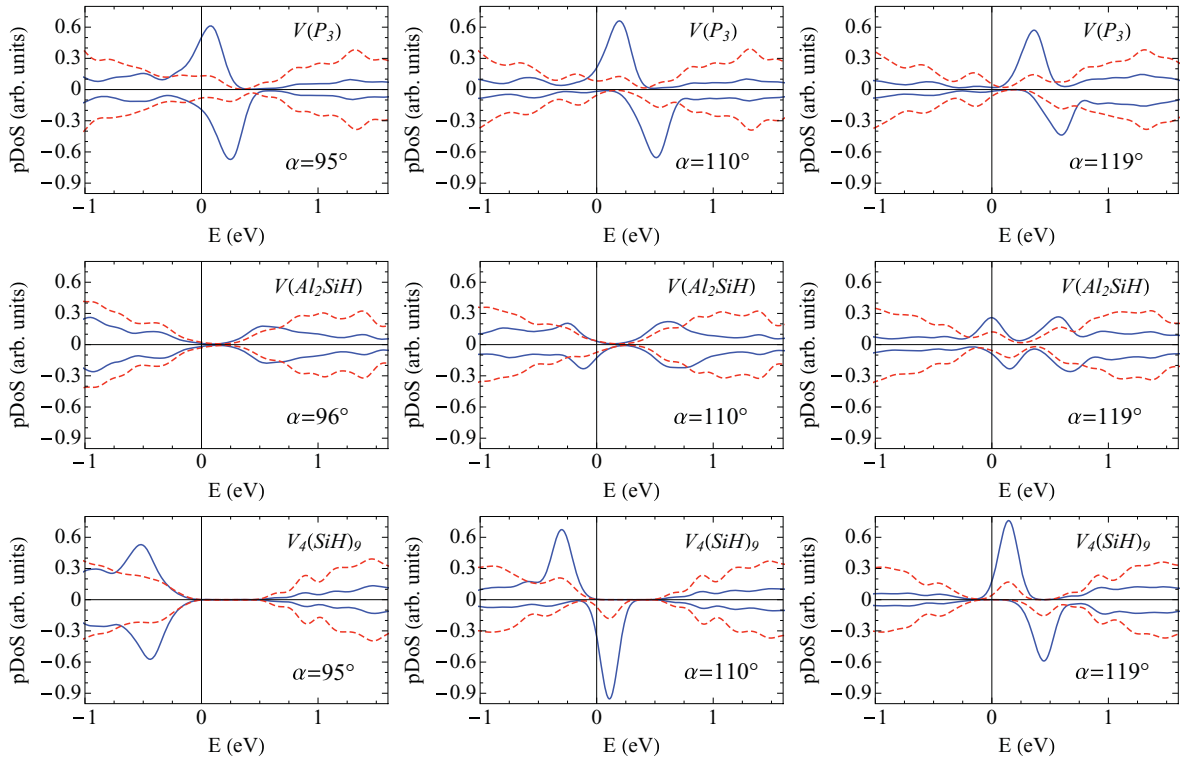

FIG. 4. (Color online) Projected density of states $D(E)$ for three different bond angles for the $V(Al_2SiH)$, $V(P_3)$, and the $V_4(SiH)_9$ model, respectively. For clarity, we plot $D^{\uparrow}(E)$ and $-D^{\downarrow}(E)$, respectively. The dashed line indicates the scaled total density of states (scaling factor 0.035). The energies are aligned to the valence-band maximum of c-Si.

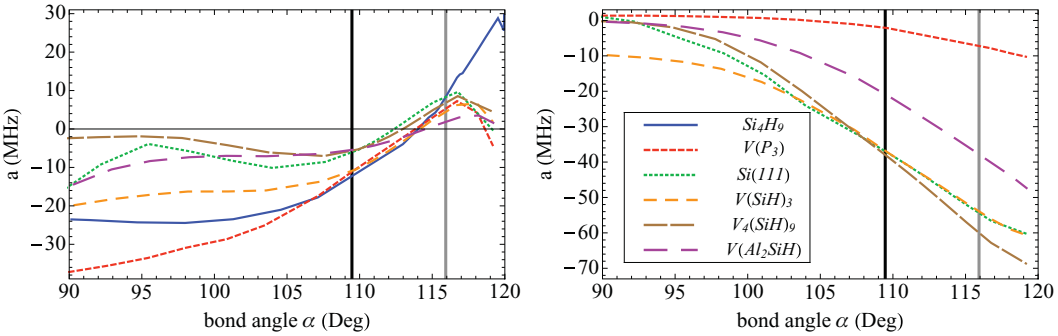

FIG. 5. (Color online) Dependence of the hyperfine parameters on the variation of the bond angle for the backbond neighbors of the Si_4H_9 molecule as well as for the c-Si db models [a: Si_4H_9, b: $V(P_3)$, c: Si(111), d: $V(SiH)_3$, e: $V_4(SiH)_9$, f: $V(Al_2SiH)$]. The black line marks the bond angle of the c-Si db models and the gray line marks that of the Si_4H_9 molecule, respectively.

the hyperfine parameters and the bond-angle range with respect to this aspect. For that we consider again amorphous silicon, for which theory[33,34] and experiment[31,35,36] estimate bond-angle variations of up to 15°. Considering an interval of ±10% around the tetrahedral bond angle, one obtains the following trends for the change of a and b. Within a non-self-consistent, single-site LCAO model,[12] where the dangling bond is restricted to the undercoordinated Si atom only, the isotropic parameter varies by 60%–90% and the anisotropic parameter by 20%–33% within the chosen bond-angle interval. In comparison, we get from our calculations for a delocalized defect, i.e., the $V(Al_2SiH)$ model, a variation on the order of ±35% for the isotropic parameter and ±25% for the dipolar coupling. On the other hand, for a localized model, i.e., $V(P_3)$, there are dramatic fluctuations of the hyperfine parameters with bond angle, namely by 20%–65% for the a parameter and by 5%–45% for the b parameter respectively. This quantitatively illustrates that the hyperfine parameters are more sensitive to changes in the local structure for deep-level defects. Furthermore, it shows that the single-site LCAO model overestimates the change of the isotropic coupling as well as the one of the anisotropic coupling for large bond angles. In turn, this means that this simple model predicts a smaller bond-angle range for a given interval in a compared to self-consistent calculations.

V. SUPERHYPERFINE COUPLING

The analysis of the superhyperfine interaction yields further information about the defect, such as its coordination in amorphous silicon.[37,38] For that reason, we consider the bond-angle dependence of the first and second nearest neighbors of the c-Si models (Fig. 5). Here we focus on the isotropic coupling, which is a measure for the spin distribution within the network.

The first neighbors show the following trends. For small bond angles, a large coupling is obtained for the localized defects. With increasing bond angle, one observes a change from majority to minority spin density, which is almost independent of the model. This has been observed before in the context of small-molecule systems[7] and can be explained by spin-polarization effects. On the other hand, the second neighbors show a continuous increase of a for larger bond angles, i.e., as more spin density is pressed into the network. Consequently, the isotropic coupling of these atoms is directly related to the geometry of the defect. However, the magnitude depends on the chemical environment being largest for the hydrogen-saturated vacancies. In all models, with the exception of $V(P_3)$, the larger second-neighbor coupling exceeds the first-neighbor one, which has been also observed previously.[7,39]

Besides the backbond couplings, there is also a significant isotropic coupling for atoms opposite the db atom, which has not be observed in previous cluster models [Table II and Fig. 1(b)]. Those atoms are at the same distance as the second nearest neighbors and are attached to a hydrogen atom. As one can see from Table II, the hyperfine parameters of the opposite atoms are very close to the ones of the second nearest neighbors in the backbond direction. From this we can conclude that the network, i.e., the connection of an atom to the db atom via bonds, is not a necessary condition for the spin distribution. Therefore, it may be difficult to resolve the different positions experimentally. We therefore conclude that the common assumption that a significant superhyperfine interaction occurs only in the backbond atoms[7,11,12] needs to be revised.

TABLE II. Isotropic/dipolar hyperfine parameters (in MHz) of various hydrogenated vacancies. The parameters are shown for the db atom, second-nearest neighbors, as well as Si atoms opposite the db atom at the same distance as the second-nearest neighbors (3.81 Å).

a/b (MHz)	$V(SiH)_3$	$V_2(SiH)_5$	$V_3(SiH)_7$	$V_5(SiH)_{11}$
Si-db	−345/−48	−33/−6	−24/−3	−396/ − 53
2nd neighbor	−33/ − 6	−37/ − 6	−37/ − 6	−37/ − 6
opposite Si-H	−24/ − 3	−39/ − 4	−37/ − 4	−37/ − 4

VI. CONCLUSIONS

We have analyzed the dependence of the hyperfine parameters of the silicon dangling-bond defect on bonding parameters. For that purpose, we have carried out systematic *ab initio* studies for small clusters and for crystalline supercell models. These models capture in particular the effect of delocalization, which has been neglected in previous studies. Bond-length variations induce a linear trend for the isotropic parameter but hardly affect the anisotropy. The dependence of the hyperfine parameters on the bond angle turns out to be more complex. For deep-level defects, one observes trends that are in agreement with the s-p hybridization picture. However, if the defect state approaches the valence-band edge, hybridization occurs and leads to a delocalization of the unpaired electron. This delocalization can be induced by the chemical surrounding but also by the geometry of the defect. From the observed trends we conclude that the hyperfine parameters can only characterize the local structure of sufficiently deep defects. For less localized cases, the relation between local geometry (degree of s-p hybridization) and hyperfine couplings becomes increasingly modified by additional factors such as the chemical environment, local charges in the vicinity, or the interaction with nonbonded residues (e.g., hydrogen) nearby. This implies that bond parameters cannot be reliably deduced from measured hyperfine couplings alone if delocalized defects dominate or even only contribute to the observed hyperfine distribution. Rather, a comparison to explicit theoretical calculations of the hyperfine parameters is needed to confirm the interpretation. These calculations must appropriately represent the extended host and its electronic structure to capture delocalization effects. Moreover, our bulk-embedded defect calculations reveal that a large superhyperfine interaction can occur at atoms opposite to the dangling bond and is not restricted to second neighbors only, as has been previously assumed by analogy to dangling-bond defects at surfaces or interfaces. Consequently, the environment opposite to the dangling bond plays in general a more important role, notably for delocalization effects, than previously recognized.

Our results also have important consequences for the interpretation of EPR experiments for the dangling bond in a-Si:H. The fundamental mechanisms of s-p hybridization and delocalization are certainly active in the amorphous case, and may serve to rationalize the effects for an individual defect configuration. However, the strong site-to-site variations, not only of the geometry and energetic position but also of the nearby environment, will hinder a direct interpretation of ensemble averages in terms of a single or averaged defect parameter. Rather, changes in the observed properties upon varying the experimental conditions could reveal the underlying effect and shed more light on the origin of the EPR signal.

ACKNOWLEDGMENTS

This work was supported by the German Ministry of Research and Education in the BMBF research project "EPR Solar" (03SF0328F), and we are greatly indebted to K. Lips, A. Schnegg, M. Fehr, C. Teutloff, and U. Gerstmann for fruitful discussions.

[1] J. A. Weil and J. R. Bolton, *Electron Paramagnetic Resonance* (Wiley, New Jersey, 2007).
[2] J. M. Spaeth and H. Overhof, *Point Defects in Semiconductors and Insulators* (Springer, Berlin, 2003).
[3] M. Kaupp, M. Bühl, and V. G. Malkin, *Calculation of NMR and EPR Parameters* (Wiley, Weinheim, 2004).
[4] T. Umeda, Physica B **376**, 249 (2006).
[5] C. Van de Walle and P. E. Blöchl, Phys. Rev. B **47**, 4244 (1993).
[6] A. Stirling, A. Pasquarello, J.-C. Charlier, and R. Car, Phys. Rev. Lett. **85**, 2773 (2000).
[7] M. Cook and C. T. White, Phys. Rev. B **38**, 9674 (1988), and references therein.
[8] A. Stesmans, B. Nouwen, and V. V. Afanas'ev, Phys. Rev. B **58**, 15801 (1998).
[9] M. Sprenger, S. H. Muller, E. G. Sieverts, and C. A. J. Ammerlaan, Phys. Rev. B **35**, 1566 (1987).
[10] U. Gerstmann, E. Rauls, H. Overhof, and T. Frauenheim, Phys. Rev. B **65**, 195201 (2002).
[11] D. K. Biegelsen and M. Stutzmann, Phys. Rev. B **33**, 3006 (1986).
[12] T. Umeda, S. Yamasaki, J. Isoya, and K. Tanaka, Phys. Rev. B **59**, 4849 (1999).
[13] M. Cook and C. T. White, Semicond. Sci. Technol **4**, 1012 (1989).
[14] A. H. Edwards and W. B. Fowler, Phys. Rev. B **41**, 10816 (1990).
[15] N. Ishii and T. Shimizu, Solid State Commun. **102**, 647 (1997), g-tensor calculation for a-Si:H.
[16] S. Blügel, H. Akai, R. Zeller, and P. H. Dederichs, Phys. Rev. B **35**, 3271 (1987).
[17] R. M. Martin, *Electronic Structure* (Cambridge University Press, Cambridge, 2004).
[18] J. Kohanoff, *Electronic Structure Calculations for Solids and Molecules* (Cambridge University Press, Cambridge, 2006).
[19] M. Fuchs and M. Scheffler, Comput. Phys. Commun. **119**, 67 (1999).
[20] B. Meyer, K. Hummler, C. Elsasser, and M. Fahnle, J. Phys. C**7**, 9201 (1995).
[21] J. R. Trail and D. M. Bird, Phys. Rev. B **60**, 7863 (1999).
[22] S. Boeck, C. Freysoldt, A. Dick, I. Ismer, and J. Neugebauer, Comput. Phys. Commun. **182**, 543 (2010).
[23] J. P. Perdew and A. Zunger, Phys. Rev. B **23**, 5048 (1981).
[24] M. Battocletti, H. Ebert, and H. Akai, Phys. Rev. B **53**, 9776 (1996).
[25] R. H. Luchsinger, Y. Zhou, and P. F. Meier, Phys. Rev. B **55**, 6927 (1997).
[26] U. Gerstmann and H. Overhof, Physica B **273**, 88 (1999).
[27] J. P. Perdew, K. Burke, and M. Ernzerhof, Phys. Rev. Lett. **77**, 3865 (1996).
[28] D. R. Hamann, Phys. Rev. B **40**, 2980 (1989).
[29] M. J. Frisch *et al.*, *Gaussian 03, Revision D.01* (Gaussian, Inc., Wallingford, CT, 2004).
[30] H. J. Monkhorst and J. D. Pack, Phys. Rev. B **13**, 5188 (1976).

[31] K. Laaziri, S. Kycia, S. Roorda, M. Chicoine, J. L. Robertson, J. Wang, and S. C. Moss, Phys. Rev. B **60**, 13520 (1999).
[32] A. Stirling and A. Pasquarello, J. Phys. Chem. A **109**, 8385 (2005).
[33] R. Singh, S. Prakash, N. N. Shukla, and R. Prasad, Phys. Rev. B **70**, 115213 (2004).
[34] K. Jarolimek, R. A. de Groot, G. A. de Wijs, and M. Zeman, Phys. Rev. B **79**, 155206 (2009).
[35] M. Wakagi, K. Ogata, and A. Nakano, Phys. Rev. B **50**, 10666 (1994).
[36] P. Roura, J. Farjas, and P. Roca i Cabarrocas, J. Appl. Phys. **104**, 073521 (2008).
[37] J. H. Stathis, Phys. Rev. B **40**, 1232 (1989).
[38] N. Ishii and T. Shimizu, Phys. Rev. B **42**, 9697 (1990).
[39] U. Gerstmann, M. Rohrmüller, F. Mauri, and W. G. Schmidt, Phys. Status Solidi C **7**, 157 (2010).